RSC Advances

ROYAL SOCIETY OF CHEMISTRY

www.rsc.org/advances

RSC Advances

COMMUNICATION

Effect of pore-size distribution in cathodic gas diffusion layer on electricity generations of microbial fuel cells (MFCs)

Received 00th January 20xx,
Accepted 00th January 20xx

DOI: 10.1039/x0xx00000x

www.rsc.org/

Xinxin Shi*, Tinglin Huang

Abstract: A simple approximate proportional relationship was found between the increases of electricity generation of microbial fuel cells and the volume fraction of mesopores in gas diffusion layers. More importantly, the underlying mechanism of the effect of pore-size distribution was explored in detail by introducing Knudsen gas transport theory.

1. Introduction

Microbial fuel cells (MFCs) are emerging technologies for extracting electrical energy from biomass, especially from pollutants in wastewater.[1] In a typical MFC, electrochemically active bacteria on the anode gain energy from metabolizing pollutants in wastewater and release the resulting electrons and protons to the cathode (electrons flowing through external circuit and protons diffusing through the electrolyte). These electrons and protons react with oxidant on the cathode and form a cell loop.[2] The single chambered air-cathode microbial fuel cells (ACMFCs) are one kind of MFCs, which use oxygen (O_2) from air as the oxidant at the cathodes and become a promising configuration of MFCs to be scaled up for wastewater treatment due to its high power output, simple structure, and no cost of electron acceptor.[3]

Reaction rate of oxygen reduction (ORR) in the cathode of MFC is almost unobservable without catalysts. Although the Pt/C as catalyst for ORR is effective, its disadvantage of high cost has greatly limited its application. The searching for its low-cost substitutes has become a hot research spot with many successful attempts such as active carbon catalyst[4, 5] and nitrogen doped carbon catalyst[6, 7]. On the other hand, rate of oxygen transport in the cathode is found to be another key factor greatly impacting the rate of ORR. Fornero et al.[8] increased the maximum power density (MPD) of MFC by 70% with a twice air pressure. Similarly, Jang et al.[9] increased the current density by 2.5 times with a 4 times enhanced aeration flux. Although these approaches are effective in improving power output, a power supply is indispensable when running MFC. Recently, the pore structure of catalyst layer was found to be critical for the improvement of ORR rate. The MPD of an ACMFC increases with the increasing of either specific surface area[10] or porosity[11] of catalyst layer. However, as the first channel of the air going through the cathode, the pores in the gas diffusion layer (GDL) might be as important as that in the catalyst layer for oxygen transport, which has received rare research attentions. In the limited literature, Cheng et al.[12] investigated the effect of the number of PTFE layers on the MPD, and showed that 4-layer GDL resulted in the largest MPD. The GDLs with more or less layers both decreased the MPD. Similar result was obtained by Zhang et al.[13] with PTFE-GDL replaced by (polydimethylsiloxane/carbon)-GDL. Yang et al[14] improved the porosity of GDLs by doping carbon black, with a 25% increase of the MPD achieved, but the effect of pore size distribution was not included.

The purpose of this work was to investigate the effect of the pore-size distribution of GDL on the MPD of MFCs. These GDLs with specific pore-size distributions were obtained by simply using different cooling methods. Then the performances of MFCs were tested and the internal resistances and overpotentials were analyzed. More importantly, the underlying mechanism of pore-size distribution effect was explored in detail by introducing Knudsen gas transport theory.

2. Materials and methods

2.1 Cathode preparation

The carbon cloth (30% wet proofed, BASF, USA) was used as the support material, with one side covered by the catalytic layer and the other side first by the carbon base layer and then by the GDLs. In the catalytic layer, nitrogen-doped carbon powders (15mg/cm^2)[7] were used as the ORR catalyst and Nafion solution (5%, 100μl/cm^2, Hesen, China) as the

School of Environmental and Municipal Engineering, Xi'an University of Architecture and Technology, Xi'an 710055, People's Republic of China Email: shixinxin@xauat.edu.cn

† Electronic Supplementary Information (ESI) available: [pore size distribution of gas diffusion layer and detailed data of electrochemical test]. See DOI: 10.1039/x0xx00000x

binder. The diffusion layer was prepared by repeating the following three steps four times: first paste carbon base layer with PTFE (60%, Hesen, China), then calcine the electrode at 370°C for 15min and finally cool the electrode.

After a series of pretests, with 370°C as the temperature of the muffle furnace set, the GDLs with different pore size distribution were prepared by adopting four different cooling procedures: (a) in refrigerator at 4°C (GDL-A); (b) in freezer at -20°C (GDL-B); (c) in muffle furnace (cooling rate: 0.5°C /min, GDL-C); (d) at room temperature (25°C, GDL-D).

2.2 MFC configuration and operation

A single-chambered cubic-shaped MFC reactor was constructed as in the work of Dong et al.[11] with a total volume of 28ml. Hydrophilic carbon cloth (BASF, USA) was used as the anode, and four types of cathodes were prepared with GDL-A, B, C and D respectively. Both the anode and cathode had a projected surface area of 7 cm^2. Reactors were operated in fed-batch mode in a constant temperature room (30 ± 1°C) with a 1000Ω external resistor and the substrate was refreshed once the voltage reduced below 20mV. All the tests were performed in triplicate.

When initializing the MFCs, the anodes were inoculated with 1:1 mixture of domestic sewage (COD = 500-600mg/l, pH = 7.0, from urban drainage system of residential district in Harbin) and phosphate buffer solution (PBS, 50mM). Glucose (1g/l) was added to the mixture as the energy source. Until the maximum voltage of the reactor in each cycle became stable, the above mixture was changed to a nutrient solution containing glucose (1g/l), PBS (50mM), vitamins (5ml/l) and minerals (12.5ml/l).[15]

2.3 Method and analysis

Polarization curves and cell voltages The polarization curve was tested by using a potentiostat (WMPG1000, Korea) with a three-electrode system (scanning rate, 0.1mV/s), and then the power density was calculated from the polarization data. The three-electrode system, immersed in 50mM PBS solution, was composed of a platinum mesh (4cm^2) as the auxiliary electrode, an Ag/AgCl electrode as the reference electrode and a cathode as the working electrode. The cell voltages were collected by a data acquisition system (PISO-813, ICP DAS Co., Ltd.) which was connected in parallel to the cell.

Electrochemical impedance spectrum (EIS) The EIS were performed with an AC signal (amplitude 10mV) ranged from 100kHz to 10mHz.[11] The cathode impedance spectra were recorded under the condition of open circuit using the cathode as the working electrode, Ag/AgCl electrode as the reference electrode and the anode as the counter electrode. The equivalent circuit as shown in Fig. S1 was used to describe the cathodic ORR and the three parameters (R_{ohm}: the ohmic internal resistance, R_c: the charge transfer resistances and R_d: the diffusion resistance) are identified by the least-squares fitting of the Nyquist plot in ZsimpWin (Ver 3.10) program.

Pore size distributions The volumes of pores with different diameters in a GDL were determined by Brunauer-Emmett-Teller (BET) adsorption isotherm tests (ASAP 2020 M, Micromeritics Instrument Corporation, USA).

Scanning electron microscope (SEM) SEM (FEI model XL30, tungsten filament, 10 KeV electron beam) was used to examine the morphology of GDLs. The cathodes were dried and then sputtered with gold particles for SEM imaging.

3. Results

3.1 Pore size distributions of GDLs

As shown by SEM images (Fig. 1), the pore structure was indeed changed by simply controlling the cooling rate. In order to quantify the pore size distributions, the volumes of micropores, mesopores, and macropores (according to the pore size classification of International Union of Pure and Applied Chemistry (IUPAC)) were calculated based on the Barett-Joyner-Halenda (BJH) adsorption pore distribution (Table 1). The BJH data showed that the total pore volumes of the four kinds of GDL were basically the same. However, there was notably different for the four kinds of cathode in terms of the ratio of the mesopore and the total pore volume (V_{meso}/ V_{total}) and the ratio of the micropore and the total pore volume (V_{micro}/ V_{total}). The values of V_{meso}/ V_{total} from high to low were as follows: GDL-D > GDL-C > GDL-B > GDL-A, with more than 20% percentage difference between the highest and the lowest. Moreover, the value of V_{micro}/ V_{total} for GDL-D was only one third or one fourth of those for the other three GDLs. The detailed data on volumes of different pore diameters was listed in Table S1. Normally, PTFE contracts with decreasing temperature. And such contraction will increase the diameters of some pores while decreasing the pore sizes of others at the same time, as shown in Fig. S2. In this process, the transition may occur from any one type of pore to the other two types, so it is very challenging to quantitatively or even qualitatively determine whether the content of a certain type of pore increases or decreases in a cooling process. For this reason, the relationship between the temperature and the volume fraction of a type of pore should be much more complex than a simple proportional relation.

Table 1 Volumes of micropores, mesopores and macropores in different GDLs

	V_{total} (m^3/g)	V_{micro} (m^3/g)	V_{meso} (m^3/g)	V_{macro} (m^3/g)	V_{micro}/ V_{total} (%)	V_{meso}/ V_{total} (%)	V_{macro} / V_{total} (%)
GDL-A	1.3×10^{-3}	2.5×10^{-4}	3.1×10^{-4}	7.5×10^{-4}	19.2	23.8	57.7
GDL-B	1.3×10^{-3}	3.5×10^{-4}	5.0×10^{-4}	4.7×10^{-4}	26.9	38.5	36.9
GDL-C	2.0×10^{-3}	5.1×10^{-4}	8.3×10^{-4}	6.2×10^{-4}	25.5	41.5	31.0
GDL-D	1.4×10^{-3}	8.3×10^{-5}	6.5×10^{-4}	6.4×10^{-4}	5.9	46.4	45.7

V_{micro},V_{meso} and V_{macro} respectively represent the volumes of micropore, mesopore and macropore.

Micropore (IUPAC): pore diameter ≤ 20Å

Mesopore (IUPAC): 20 Å <pore diameter ≤500 Å

Macropore (IUPAC): 500 Å <pore diameter

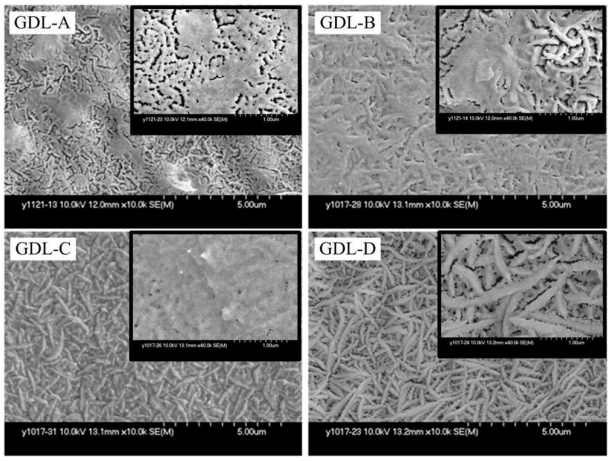

Fig. 1 SEM images of gas diffusion layers with different pore-size distributions (magnification: 10000 for the main figures and magnification: 40000 for the inset figures)

3.2 Electricity generations of MFCs with different GDLs

An obvious proportional relationship was found between the increases of MPDs and the volume fractions of mesopores in GDLs. The MPD order was consistent with the mesopore volume fractions and from high to low was as follows: GDL-D > GDL-C > GDL-B > GDL-A (Fig. 2a). The value of V_{meso}/ V_{total} of GDL-D was about twice than that of GDL-A and the MFC with GDL-D showed an 11% larger MPD than that with GDL-A, and it also persisted in a dramatically broader range at relative high current density and cell voltage (Fig. 2b, Fig. 2c and Fig. S3). In a word, the MFC with the mesopores dominated GDL (i.e. GDL-D in this paper) exhibited the largest power output.

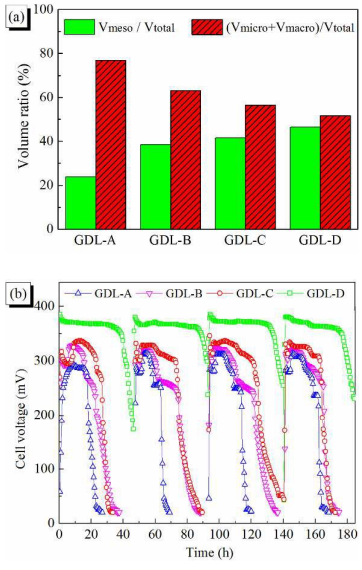

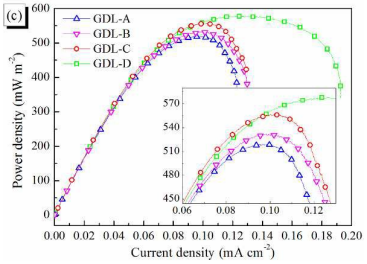

Fig. 2 Pore volume ratios of GDLs with different pore-size distributions (a), cell voltages (b), power densities (c) of MFC with different GDLs

However, it seemed unreliable to interpret the performances of GDLs and corresponding MFCs by using volume content of either micropore or macropore, because an obvious relationship wasn't observed between these two types of volume contents and the MPDs. A proportional relationship was found between micropore volume content and the MPDs in the comparison of GDL-A with GDL-D, but this is not the case in the comparison of GDL-A with GDL-C.

3.3 Losses of concentration polarization under different GDLs

Polarization test (Fig. 3a) showed that it was the gas transport overpotential ($\eta_{conc.}$) that greatly influenced by the pore size distribution of GDL, while ohmic overpotential (η_{ohm}) and charge transfer overpotential ($\eta_{act.}$) were nearly unaffected. Consequently, the GDL with mesopore dominated and micropore minimized had the minimum diffusion resistance (R_d, 15Ω), which was only about 5% of the other diffusion resistances (300-450Ω, Fig. 3b and Fig. S4).

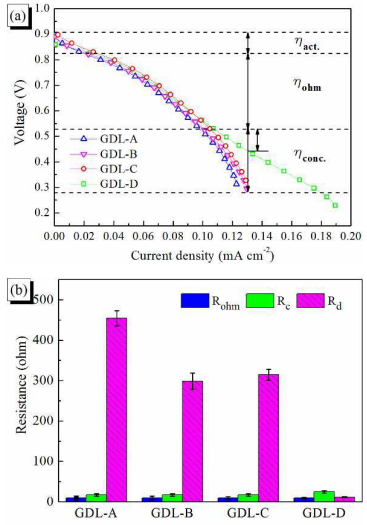

Fig. 3 Polarization curves of MFCs (a) and internal resistances of cathodes (b) using GDLs with different pore-size distributions (Rohm: ohmic resistance; Rc: charge transfer resistance; Rd: diffusion resistance)

4. Discussion

The existence of macropores was prone to causing cathodic flooding, while micropores tended to deteriorate the oxygen transport rate. In both cases the diffusion resistances would probably be too large to achieve a satisfactory power output. Attempts had been made here to quantify the relationship between pore structure and mass transport rate.

The one-dimensional diffusion of gas molecules in porous media involves molecular interactions between gas molecules as well as collisions between gas molecules and the porous media.[16, 17] As gas molecules travel through the porous media, one of three mechanisms can occur, depending on the characteristic of the diffusing gas species and the intrinsic microstructure of the porous media. The three mechanisms are molecular diffusion, viscous diffusion, and Knudsen diffusion. To distinguish among the three mechanisms, the Knudsen number (K_n) is typically used, as shown in Eq. 1

$$K_n = \frac{k_B T}{\sqrt{2} p \pi d_g^2 d_p} \quad \text{(Eq. 1)}$$

where d_p is the diameter of the pores, P is the gas pressure, d_g is the effective diameter of a gas molecule, K_B is the Boltzmann constant (1.3807×10^{-23}J/K), and T is the temperature of the gas (K).[18]

If K_n is smaller than 0.1, collisions and interactions between gas molecules become dominant, and Knudsen diffusion becomes negligible compared with molecular diffusion and viscous diffusion (Fig. 4a). If K_n is greater than 10, collisions between gas molecules and the porous electrode are more dominant than the collisions between gas molecules, resulting in negligible molecular diffusion and viscous diffusion (Fig. 4b). As K_n of a system ranges between 0.1 and 10, all three mechanisms govern gas transport (Fig. 4c).[19]

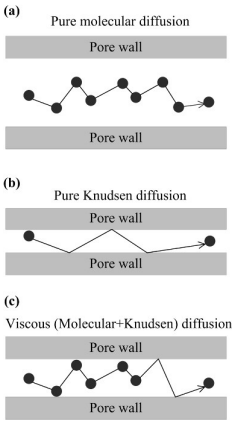

Fig. 4 Basic mechanisms of gas diffusion in porous media[18]

Given the d_g of air as 4×10^{-10}m, P as 101.325kPa, and T as 298.15K, the dominant gas transport mechanism can be determined for a certain pore size (d_p) according to Eq. 1. Thus, it can be calculated that the Knudsen diffusion dominated in the micropores, while the viscous diffusion dominated in both mesopores and macropores. For readers' convenience, a schematic diagram (Fig.5) was added for the correspondence between the GDL pore scale and the Knudsen-number-based gas diffusion modes.

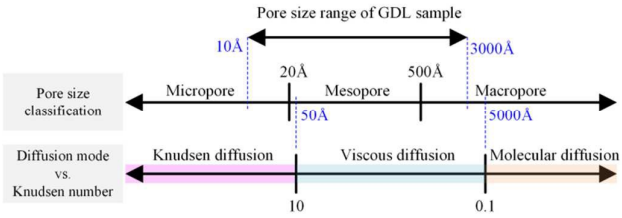

Fig. 5 Schematic diagram of the correspondence between GDL pore scale and Knudsen-number-based gas diffusion mode

The calculation based on Knudsen theory revealed that the gas transport in micropores was dominated by Knudsen diffusion (as in the case of GDL-B), so most of gas kinetic energy was consumed on the collisions between the gas molecules and the pore wall, with only a small amount of gas arriving at the catalytic layer to take part in the ORR. It should be noted that while micropores should be avoided in the GDLs, they were desired in the catalyst layers (CLs)[20]. Because the collisions between gas molecules and pore walls were desired as many as possible in order for the catalysts in the CLs to function more efficiently. This helped to explain the experimental results achieved, but without explanation, in the recent study by Dong et al. [20] that micropores were favored in CLs.

GDL-A exhibited the poorest power generation, because flooding, an important limiting factor of fuel cell performance[21], probably happened due to the largest macropore content in GDL-A. However, the test or visualization of the flooding in a cathode, especially in a GDL alone, was still challenging in the research field of MFCs. To our best knowledge, the pore size at which flooding happens, although of great research significance, has not been reported so far. For this reason, the happening of flooding in existing studies was still a reasonable guess used to explain the low MPDs when a cathode was prepared with GDL of large pore size[22, 23] or was exposed to wet air[24].

Mesopores prevented the happening of flooding while ensuring a good gas transport due to the viscous diffusion. Thus the larger the mesopore content, the faster gas transport as well as the higher MPDs could be expected. This was confirmed by the relationship between the mesopore volume fractions and the MPDs observed in all the four GDLs (Fig.2 (a) and (c)).

Conclusions

Experimental results showed that the content of micropore determined the diffusion resistance and macropores tended to causing cathodic flooding. However, the content of mesopore volume was found to be a reliable way for interpreting the performances of GDLs. The underlying mechanism of the effect of pore-size distribution can be well

explained with the help of Knudsen related gas transport theory. The theory also resulted in a fundamental principle that mircropores should be avoided in the GDLs, while they are desired in catalytic layers in which more collisions between gas molecules and pore walls leads to a more efficient catalysis.

Acknowledgements

This research was supported by the National Natural Science Foundation of China (No.51408469) and by the Key Laboratory of Education Department of Shaanxi province (15JS046) and Xi'an University of Architecture and Technology (QN1416 and RC1366).

References

1 B. Logan, S. Cheng, V. Watson and G. Estadt, *Environ Sci Technol*, 2007, **41**, 3341-3346.
2 S. K. Chaudhuri and D. R. Lovley, *Nat Biotechnol*, 2003, **21**, 1229-1232.
3 A. Dewan, H. Beyenal and Z. Lewandowski, *Environ Sci Technol*, 2008, **42**, 7643-7648.
4 S. Cheng and J. Wu, *Bioelectrochemistry*, 2013, **92**, 22-26.
5 F. Zhang, S. Cheng, D. Pant, G. Van Bogaert and B. E. Logan, *Electrochem Commun*, 2009, **11**, 2177-2179.
6 L. Feng, Y. Yan, Y. Chen and L. Wang, *Energ Environ Sci*, 2011, **4**, 1892-1899.
7 X. Shi, Y. Feng, X. Wang, H. Lee, J. Liu, Y. Qu, W. He, S. S. Kumar and N. Ren, *Bioresource Technol*, 2012, **108**, 89-93.
8 J. J. Fornero, M. Rosenbaum, M. A. Cotta and L. T. Angenent, *Environ Sci Technol*, 2008, **42**, 8578-8584.
9 J. K. Jang, T. H. Pham, I. S. Chang, K. H. Kang, H. Moon, K. S. Cho and B. H. Kim, *Process Biochem*, 2004, **39**, 1007-1012.
10 X. Zhang, X. Xia, I. Ivanov, X. Huang and B. E. Logan, *Environ Sci Technol*, 2014, **48**, 2075-2081.
11 H. Dong, H. Yu, X. Wang, Q. Zhou and J. Feng, *Water Res*, 2012, **46**, 5777-5787.
12 S. Cheng, H. Liu and B. E. Logan, *Electrochem Commun*, 2006, **8**, 489-494.
13 F. Zhang, T. Saito, S. Cheng, M. A. Hickner and B. E. Logan, *Environ Sci Technol*, 2010, **44**, 1490-1495.
14 W. Yang, F. Zhang, W. He, J. Liu, M. A. Hickner and B. E. Logan, *J Power Sources*, 2014, **269**, 379-384.
15 H. Liu and B. E. Logan, *Environ Sci Technol*, 2004, **38**, 4040-4046.
16 M. Cannarozzo, A. Del Borghi and P. Costamagna, *J Appl Electrochem*, 2008, **38**, 1011-1018.
17 J. W. Veldsink, R. Van Damme, G. F. Versteeg and W. Van Swaaij, *The Chemical Engineering Journal and the Biochemical Engineering Journal*, 1995, **57**, 115-125.
18 W. He, W. Lv and J. Dickerson, *Gas Transport in Solid Oxide Fuel Cells*, Springer, 2014.
19 J. R. Welty, C. E. Wicks, G. Rorrer and R. E. Wilson, *Fundamentals of momentum, heat, and mass transfer*, John Wiley & Sons, 2009.
20 H. Dong, H. Yu and X. Wang, *Environ Sci Technol*, 2012, **46**, 13009-13015.
21 U. Pasaogullari and C. Y. Wang, *J Electrochem Soc*, 2004, **151**, A399-A406.
22 J. Joo, M. Choun, K. Kim, S. Uhm, Y. D. Kim and J. Lee, *Curr Appl Phys*, 2014, **14**, 1374-1379.
23 N. Holmström, J. Ihonen, A. Lundblad and G. Lindbergh, *Fuel Cells*, 2007, **7**, 306-313.
24 T. Hottinen, M. Noponen, T. Mennola, O. Himanen, M. Mikkola and P. Lund, *J Appl Electrochem*, 2003, **33**, 265-271.

RSC Advances

COMMUNICATION

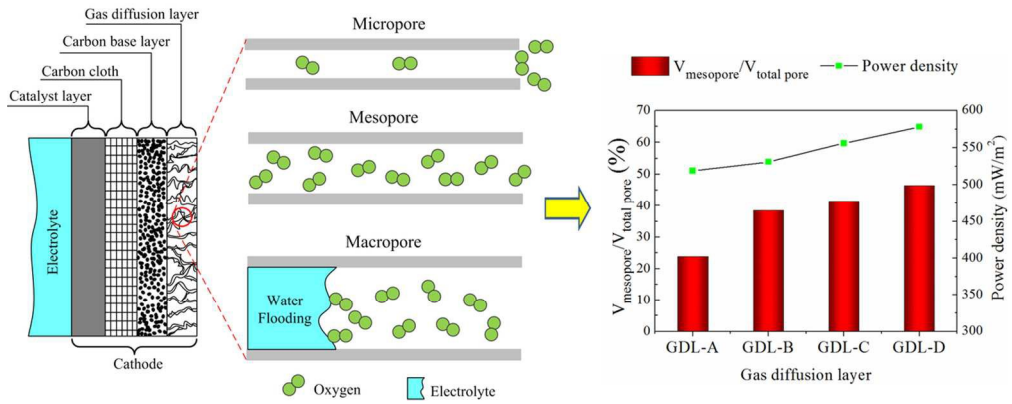

113x44mm (300 x 300 DPI)